Cement and Concrete Research 41 (2011) 865–571

Contents lists available at ScienceDirect

Cement and Concrete Research

journal homepage: http://ees.elsevier.com/CEMCON/default.asp

Influence of mineralogy on the hydraulic properties of ladle slag

Daniel Adolfsson [a,*], Ryan Robinson [b], Fredrik Engström [b], Bo Björkman [b]

[a] SSAB Merox SE-61380 Oxelösund, Sweden
[b] Luleå University of Technology Department of Civil, Environmental and Natural Resources Engineering Division of Sustainable Process Engineering, SE-97187 Luleå, Sweden

ARTICLE INFO

Article history:
Received 3 August 2010
Accepted 15 April 2011

Keywords:
Calcium aluminate cement (D)
Calorimetry (A)
Hydration (A)
Ladle furnace slag

ABSTRACT

The present study is aimed at investigating the hydraulic characteristics of ladle furnace slag (LFS), under the pretence of using LFS as a cement substitute in certain applications. Furthermore, LFS has been considered as a possible activator in a blend containing 50% LFS, and 50% ground granulated blast furnace slag (GGBFS). Phases detected in LFS were quantified using Rietveld analysis. Calorimetric studies were performed at 20, 25 and 30 °C in order to calculate the apparent activation energy of hydration and thereby to suggest a kinetic model for the tested compositions within this temperature interval. In addition, compressive strength tests were performed on mortar prisms made with LFS, and LFS/GGBFS which had hydrated for 2, 7 and 28 days. Both compositions reached acceptable early strengths, (e.g. LFS, 33.1 MPa, and LFS/GGBFS, 17.9 MPa, after 2 days), but after 28 days hydration the blend was superior to neat LFS. Related apparent activation energies were determined using an Avrami–Erofeev model and gave $E_a = 58$ kJ/mol for neat LFS and $E_a = 63$ kJ/mol for the blend. The results imply that LFS or a LFS/GGBFS blend can be favourably used as supplement in binder applications such as binder in by-product metallurgical briquettes, which are used as recycle to the blast furnace or basic oxygen furnace depending on the specific briquette composition.

1. Introduction

SSAB EMEA is a producer of high strength steels, and the main types of metallurgical slags that are produced in parallel to the production of steel are blast furnace slag (BFS), basic oxygen furnace slag (BOS) as well as ladle furnace slag (LFS), from the secondary ladle metallurgy. Different combinations of slag formers used in each of the aforementioned operation units are an important reason as to why the mineralogical composition is considerably different in each case. Ground granulated blast furnace slag (GGBFS) produced within SSAB EMEA is very amorphous, i.e. 98% glass content, due to granulation with water. GGBFS is latently hydraulic and requires activation, which is why ordinary Portland cement (OPC) is added. LFS and BOS are crystalline in character since these materials are slowly cooled at ambient temperature in the slag yard. An important difference between LFS and BOS is the high content of calcium aluminates, which are present in the LFS type of slag. Typical minerals found in the BOS are dicalcium silicate, dicalcium ferrite, manganese and magnesia analogues of wuestite as well as free lime. The refining of steel from which the LFS originates includes different process techniques depending on the steel grade. The treatment is generally associated with parameters such as deoxidation, removal of inclusions, addition of alloying elements, desulphurisation, and temperature control of the steel bath, etc. For these reasons, the chemical composition of LFS may vary, but the mineralogical composition can remain relatively stable. The main oxides are CaO, Al_2O_3, SiO_2 and MgO, but the content of MnO can also reach significant levels depending on the steel grade produced. The use of aluminium as a deoxidation agent contributes to the formation of calcium aluminates like mayenite ($C_{12}A_7$), and tricalcium aluminate (C_3A) in the solidified slag. It is generally accepted that calcium aluminates are highly hydraulic, and react very quickly with water, especially mayenite [1]. The hydration of different calcium aluminates in water results in the formation of hydrates such as C_2AH_8, C_4AH_{13}, CAH_{10}, and C_3AH_6, [2], which give strength to the material. Among these hydrates, only C_3AH_6 is thermodynamically stable [3]. Consequently, all the other hydrates eventually convert to C_3AH_6 as a final product and the conversion process can adversely affect the final strength of the material.

Although some studies on the hydraulic potential of LFS have been completed, they are comparatively limited. Recently, Setién et al. [4] characterised ladle slag for use as a construction material. Mineralogical analysis detected crystalline phases such as $C_{12}A_7$, C_3A, and polymorphs of C_2S, among others. It was further suggested that LFS can be recycled in construction and civil engineering applications. It was also concluded, however, that presence of free periclase and carbonation enables volumetric changes which should be considered carefully before the material is used in any application. LFS has also been assessed as raw material for the production of sulphoaluminate belite cement (SAB) [5]. Different mixtures of slag as well as neat LFS were fired at 1200 °C, after which the quenched SAB clinker was characterised, and the hydraulic properties evaluated. It was concluded that steelmaking slags as well as

* Corresponding author. Tel.: +46 155 25 59 62; fax: +46 155 25 58 44.
E-mail address: daniel.adolfsson@ssab.com (D. Adolfsson).

0008-8846/$ – see front matter © 2011 Elsevier Ltd. All rights reserved.
doi:10.1016/j.cemconres.2011.04.003

neat LFS have good potential as raw material for slow hardening SAB cement, [5,6]. LFS as a binder supplement in cold-bonded briquettes, containing iron and steelmaking residues, suggests an opportunity for internal cost and environmental savings at the steelworks. A partial substitution of OPC, which is traditionally used as binder in briquettes, with LFS would save costs on binder and is a more environmentally sound alternative, since it reduces LFS tonnage sent to landfill.

2. Material and experimental procedure

2.1. Material

The experiments conducted in this study are based on samples of slow-cooled LFS and super-cooled BFS originating from SSAB EMEA. The GGBFS is an amorphous material consisting of about 98% glass content due to the granulation. The chemical composition of the LFS and typical GGBFS is presented in Table 1.

2.2. Experimental procedure

A slow-cooled LFS sample of approximately 19 kg was collected at the slag yard for further processing. The material was initially crushed to <5 mm using a Jaw crusher and thereafter separated into two fractions, >0.5 mm and <0.5 mm. The >0.5 mm fraction was run through a magnetic separator to remove metal droplets, roughly 6 wt.% of the total coarse fraction. The non-magnetic fraction was recombined with the <0.5 mm size fraction, which was not run through the magnetic separation. The grinding proceeded in two steps, of which the first was carried out with a rod mill for 20 min + 20 min, followed by a second step carried out in a ball mill for 20 min + 120 min. The aim was to determine the level of d_{80} of the material. The density and specific surface were 3.17 g/cm^3 and 3500 cm^2/g, respectively. The grindability of the material was determined to be 68 kWh/ton at a level of $d_{80} \approx 50$ μm.

2.3. X-ray diffraction

Rietveld analysis was used for the quantification of phases in the LFS. The examination was performed with a STOE θ/θ-diffractometer as well as CuKα radiation (λ = 1.5418 Å), U = 40 kV, I = 40 mA, in the angle region 2θ = 5–90°. The step size was set to Δ2θ = 0.04°, and time/step = 6 s. Rietveld program SiroQuant®, Version 3.0 was used for the quantitative phase analysis. The analyses were performed by Röntgenlabor Dr. Ermrich, Germany, and the XRD pattern of the unhydrated LFS is given in Fig. 1. In this figure, the main peaks of each phase were noted. Hydrated samples of LFS from the calorimetric study were examined on a Phillips X'pert Pro diffractometer with CuKα radiation (λ = 1.5406 Å), U = 45 kV, I = 40 mA, and an X'celerator detector. The scanning was performed in the angle region 2θ = 5–70°, at Cementa Research AB, Sweden. The calorimetric analyses were completed after 24 h, after which acetone was added to the samples prior to XRD analyses in order to stop the hydration.

2.4. Scanning electron microscopy

SEM-analysis of solid solution was performed with a Phillips XL 30 SEM equipped with energy dispersive spectra in the 20 keV range. The mould prepared for SEM analysis was sputter-coated with a conductive layer of gold.

Table 1
Chemical composition of LFS and GGBFS.

Element	FeO	CaO	SiO_2	Mn_2O_3	Al_2O_3	MgO	Na_2O	K_2O	TiO_2	Total	LOI
LFS	4.8	40.0	5.0	8.1	32.5	5.9	0	0.1	0.6	96.1	2.0
GGBFS	0.4	30.2	34.2	0.8	12.9	17.3	0.5	0.5	2.2	98.8	0.9

2.5. Calorimetry

Isothermal calorimetry was performed using a thermal activity monitor (TAM) instrument and Admix ampoules. The instrument is an eight-channel heat flow calorimeter for heat flow measurements in the milliwatt range. The water for hydration of the sample was introduced and mixed in-situ in order to obtain the complete hydration curve. The (w/c)-ratio was set to 0.6 at 20, 25 and 30 °C, and the analyses were run for 24 h. The result is based on duplicate samples, and the measurement was performed by Cementa Research AB, Sweden.

2.6. Compressive strength

Mortar prisms with dimensions of 4 × 4 × 16 cm were hydrated for 2, 7 and 28 days before testing according to EN 196-1. The sand to binder ratio was 3:1 and the w/b was 0.5. During the first 24 h, the mortars were cured in a moisture chamber with 95% relative humidity at 20 °C. Thereafter, the moulds were left to cure in water at 20 °C up to the time for compression testing. Compressive strength tests were performed by Cementa Research AB, Sweden.

3. Results and discussion

3.1. Rietveld analysis

The result of quantitative XRD, (Rietveld analysis) is given in Table 2. The amount of crystalline phases was determined to be 65 wt.% of which only 60 wt.% could be assigned, i.e. the crystalline amount was normalised at 60 wt.%. The calculated error indicates an acceptable precision of the determined crystalline phases determined as the calculation at this stage is aimed at assessing only the approximate distribution of phases. The error of the whole system, however, is expected to increase as there also existed a significant amount of amorphous phase which was calculated to approximately 35 wt.%. The amorphous phase content was determined separately with a second and third XRD-run using pure quartz as an internal standard. The calculation of the amorphous phase was possible by knowing the specific wt.% of the added standard to the sample in each XRD run. The error of the determination was in the region of approximately ±5%.

The composition contains several known hydraulic phases, of which the aluminates refer to the abundant phases. Mayenite (~12 wt.%) is typically present as a minor phase in calcium aluminate cements (CAC), but appears frequently as a major constituent in Swedish ladle slags. Tricalcium aluminate, an important component of the OPC system, was present at ~9 wt.%. Other favourable minerals are: β-C_2S (~6 wt.%), which has been extensively studied in OPC; and the principal phase detected in the gehlenite group [7], known as pleochroite or Q-phase [8], often formed in high alumina cements with more than 1% of MgO [9]. The Q-phase may influence the hydraulic properties of LFS by initially forming similar hydrates to those seen in high alumina cements at room temperature, [10]. Wuestite (FeO) which is present at about 7% is actually expected to form a solid solution with manganese and magnesia. Normally, a shifting can be seen to the left or to the right depending on whether manganese or magnesia is the dominating element in the FeO structure, but there were no shifting that could be clearly discerned in the XRD result. In Fig. 2, however, the EDS-mapping with SEM clearly suggests that Fe, Mg and Mn form a solid solution. FeO and/or (Fe,Mg, Mn)O are not expected to have any important influence on the hydration properties, which is further commented on in Section 3.2. The interesting aspect of (Fe,Mg,Mn)O is that the solid solution is weakly hydraulic and will not contribute to a volume expansion like free MgO would.

3.2. Calorimetric analysis

The first six hours of hydration is represented in Fig. 3 as a function of time for each composition at the respective temperatures. The

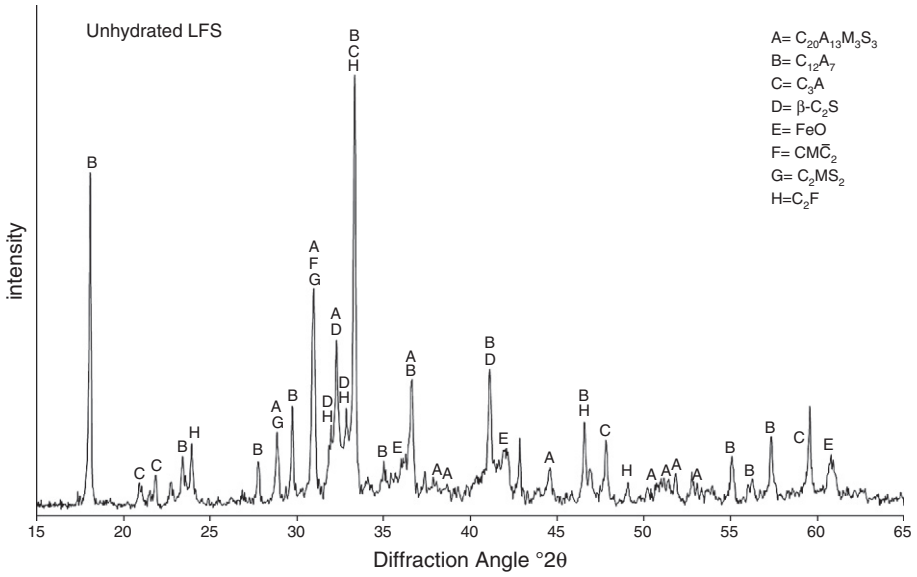

Fig. 1. Qualitative phase determination of unhydrated LFS.

course of heat evolution is characterised by three stages in terms of an initial, an induction and an acceleration period. The heat evolution that followed after the acceleration period continuously levelled off. From that point and until 24 h there was no additional increase in heat liberation that could be observed.

The setting time of $C_{12}A_7$ occurs in a few minutes [11], and cements that contain a substantial content of mayenite are reported to primarily form C_2AH_8, even at low temperatures [3]. Recalling that mayenite and tricalcium aluminate in total account for approximately 21 wt% of the crystalline phases according to Table 2, the first initial intense peak, t<1 h, is primarily associated with the wetting of the material and the dissolution of $C_{12}A_7$, C_3A as well as $CM\bar{C}_2$. The other phases that are present according to Table 2 are not expected to influence the early hydration behaviour to any major extent like mayenite and tricalcium aluminate. For instance, C_2S which reacts with water to form calcium silicate hydrates (C–S–H), is very well known from investigations of OPC to react slowly. Midgley et al. [12], has also found that β-C_2S can react with alumina gel to form stratlingite in the presence of about 10% $Ca(OH)_2$.

The hydration of wuestite (which may also be present in CAC), can lead to the formation of Fe^{2+} and Fe^{3+} hydroxide, and may become incorporated in other hydrates [2]. Åkermanite is reported to react slowly [9], and is considered as a non-cementitious phase [13]. C_2F is reactive with water, and is reported to form amorphous $Fe(OH)_3$ and C_4FH_{13} which converts to C_3FH_6 within a day, and further $Ca(OH)_2$ and haematite, [14]. The calculated content of this phase in the current study (~3 wt.%) suggests comparatively limited influence on the hydration of LFS. Pleochroite glass is reported to be weakly hydraulic [2], but there are also studies considering the MgO analogue of pleochroite, i.e. Q-phase, to be reactive [9],[10] as was mentioned earlier in Section 3.1.

In the induction period, the heat flow reaches its minimum at the time the main hydrate-growth starts, in parallel to decreasing concentrations of calcium and alumina. The hydrate growth explains the next increase in heat liberation. The acceleration period was clearly temperature dependent for both neat LFS and the blend with GGBFS and was dominated by reactions (1), [14] and (2), [2], which was confirmed by XRD analysis performed after the completion of calorimetric measurements.

$$2C_3A + 27H \rightarrow C_4AH_{19} + C_2AH_8 \quad (1)$$

$$C_{12}A_7 + 51H \rightarrow 6C_2AH_8 + AH_3 \quad (2)$$

The phases determined in Fig. 4a and b are noted as dominating phases due to significant overlap at the main peaks of the hydrates, which makes the evaluation more difficult. XRD of hydrated LFS at 20 °C, Fig. 4a, revealed formation of phases C_2AH_8 (8.2° 2θ and 16.4° 2θ), and C_4AH_{19} (8.3° 2θ and 16.7° 2θ), whereas the $C_2AH_{7.5}$ phase dominated at 25 °C with strong reflections at 8.4° 2θ, and 17.0° 2θ. The more pronounced peak of $C_2AH_{7.5}$ at 25 °C, may be explained by the conversion of C_2AH_8 to $C_2AH_{7.5}$, which was discussed in a paper by Pöllman et al. [15]. The conversion of α-C_2AH_8 to β-C_2AH_8 has also been reported by Bensted, [2]. At 30 °C, the reflection of $C_2AH_{7.5}$ overlaps with C_4AH_{19}, but is still more dominating than it was at 20 °C. There were also small peaks identified as C_2ASH_8 (7.1° 2θ and 14.2° 2θ), which tends to increase with temperature. The formation of C_2ASH_8 is an indication that Q-phase may have started to dissolve which would be in accordance with a study from Kaprálik et al. [10]. The probable contribution of pleochroite to the formation of stratlingite has been reported by Midgley et al. as well [12]. The Q-phase in the present study does persist after 24 h of hydration, but the reflections of the main peaks are reduced in comparison to those of the unhydrated LFS sample. Recalling the study by Midgley et al. [12], where they concluded that the formation of stratlingite occurred via β-C_2S, Al_2O_3 gel and approximately 10% Ca $(OH)_2$, it cannot be disregarded that the formation of stratlingite in this study may also occur along the same lines due to the reaction of dolomite. It is also possible that the amorphous phase contributes to the formation of stratlingite. From the current results, we cannot discern any dissolved quantity of either Q-phase, β-C_2S or the amorphous phase. It is,

Table 2
Rietveld analysis of LFS.

Mineral	Chemical formula	Abbreviation	Quantity in wt.%	#PDF-reference
Pleochroite/Q-phase	$Ca_{20}Al_{26}Mg_3Si_3O_{68}$	$C_{20}A_{13}M_3S_3$	20.6 ± 2.0	35-133
Mayenite	$Ca_{12}Al_{14}O_{33}$	$C_{12}A_7$	11.6 ± 1.8	1-77-5485
Tricalcium aluminate	$Ca_3Al_2O_6$	C_3A	8.9 ± 1.5	38-1429
Wuestite	FeO	f	6.6 ± 0.8	6-615
Dicalcium silicate	β-Ca_2SiO_4	β-C_2S	5.9 ± 1.1	33-302
Dolomite	$CaMg(CO_3)_2$	$CM\bar{C}_2$	3.5 ± 0.6	36-426
Dicalcium ferrite	$Ca_2Fe_2O_5$	C_2F	2.9 ± 0.4	4-7-2756
Åkermanite	$Ca_2MgSi_2O_7$	C_2MS_2	<1	1-76-7550

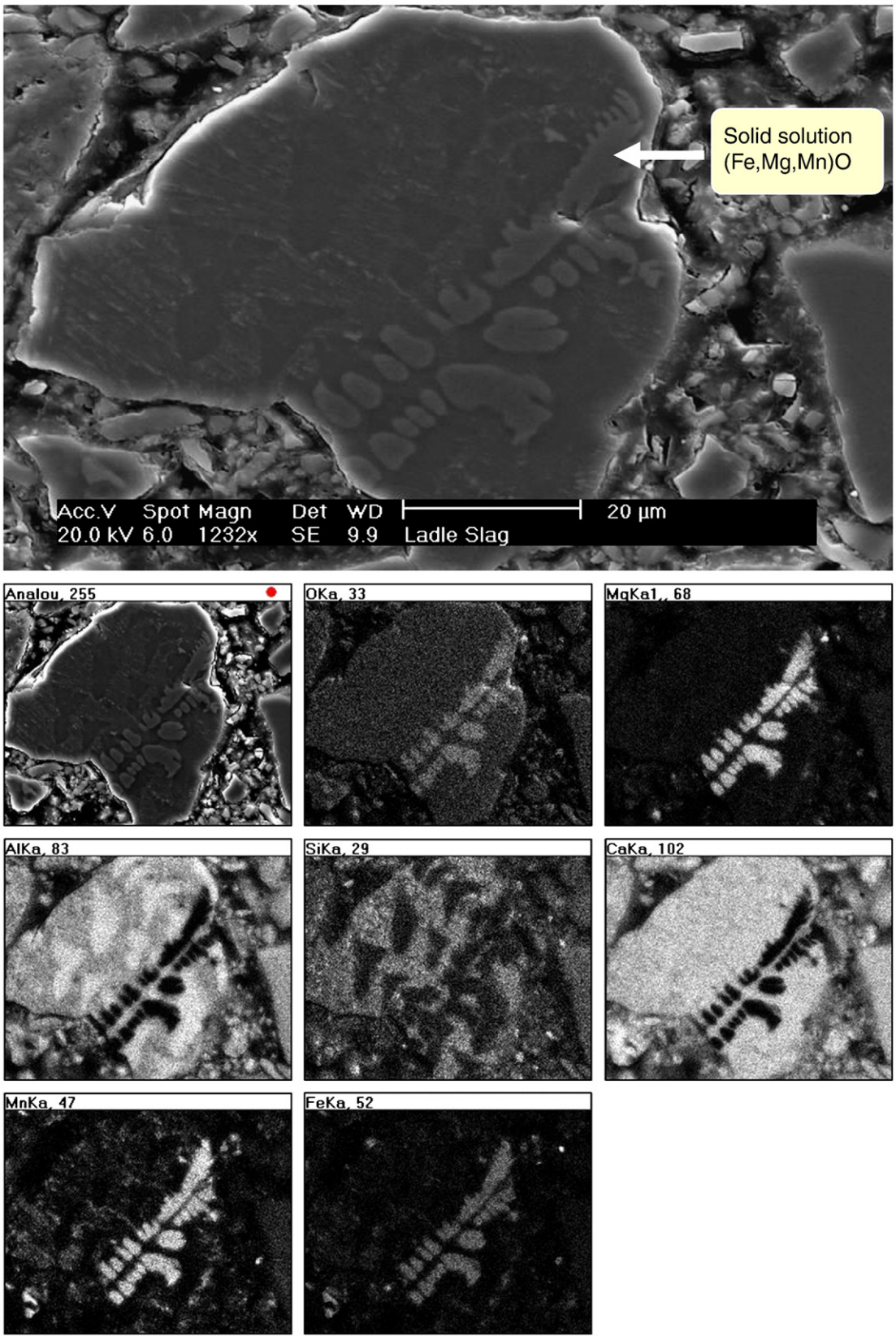

Fig. 2. SEM EDS-mapping of LFS particle containing solid solution of (Fe,Mg,Mn)O.

however, maintained that the properties of $C_{12}A_7$ and C_3A warrant more attention in any given application in the early hours of hydration since only traces of these phases are remaining along with resultant strong peaks of calcium aluminate hydrates shown in Fig. 4a. Finally, there were also traces of CAH_{10} detected at 20 °C in Fig. 4a. Fig. 4b, represents XRD results of the blend, which was much more straightforward with regard

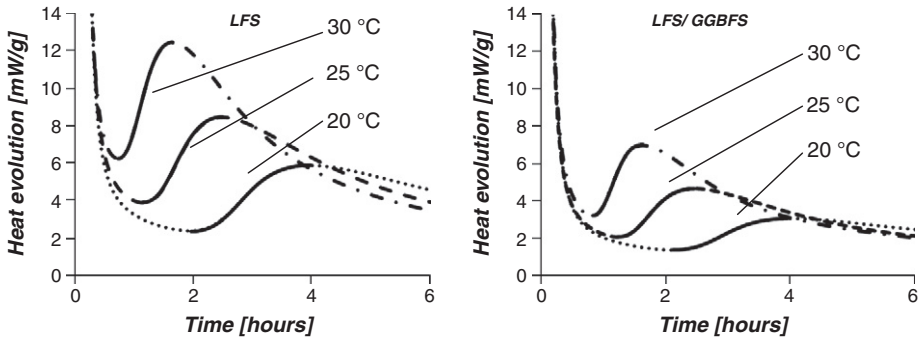

Fig. 3. Calorimetric analysis of LFS, and LFS/GGBFS at 20, 25 and 30 °C.

to the determination of hydrates. The two main hydrates detected were $C_2AH_{7.5}$ and C_2ASH_8. The fore mentioned conversion of C_2AH_8 to $C_2AH_{7.5}$ therefore seems to progress faster in a blend with GGBFS. It is also important to note that the main reference peaks of C_4AH_{19} could not be matched with any of the peaks achieved in the XRD pattern. Another considerable difference between hydrated LFS and LFS/GGBFS are the much more pronounced peaks of C_2ASH_8 in the blend which also showed significant temperature dependence. Strong peaks of C_2ASH_8 at 25 and 30 °C implies that the silica network of the GGBFS has started to react with hydrates of LFS.

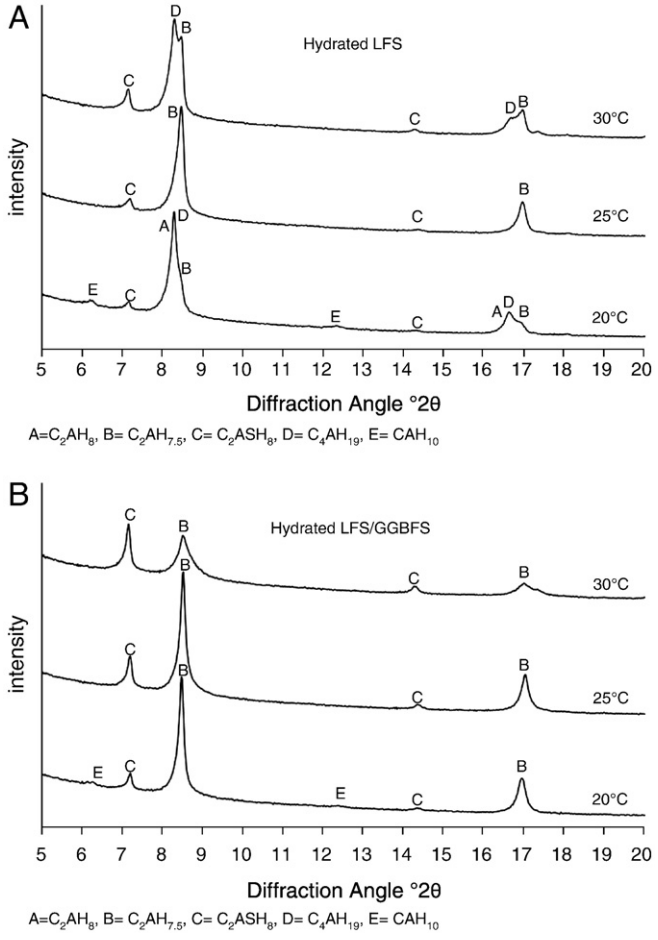

Fig. 4. a) XRD-patterns of hydrated ladle slag at 20, 25 and 30 °C, and (w/c) = 0.6. The phases determined are those considered as dominating in the sample. b) XRD-patterns of hydrated ladle slag/GGBFS at 20, 25 and 30 °C, and (w/c) = 0.6. The phases determined are those considered as dominating in the sample.

In the same figure, it can also be seen that an increase in C_2ASH_8 formation is accompanied with a decrease of the intensity of $C_2AH_{7.5}$. It therefore seems like the formation of C_2ASH_8 may proceed via $C_2AH_{7.5}$ and not necessarily C_2AH_8 as was reported in a study where calcium aluminate cement was mixed with GGBFS, [16]. There are also studies completed on mixtures of mayenite and GGBFS, [17]. Also in that case, the formation of C_2ASH_8 was suggested to form via C_2AH_8 and that C_2ASH_8 formation could occur only after a few weeks at 20 °C. In the current study, however, the formation of C_2ASH_8 appeared already after 24 h in both the neat LFS and in the blend with GGBFS. The contribution to long-term strength through the formation of C_2ASH_8 has been discussed in similar studies [2], [18], [19]. The initiated formation of C_2ASH_8 is therefore very important from the point of view that C_2ASH_8 may restrict the otherwise forthcoming conversion of $C_2AH_8/C_2AH_{7.5}$ and C_4AH_{19} to C_3AH_6.

3.3. Compressive strength tests

Mortar prisms of LFS exhibited good performance by measuring 33.1 MPa after 2 days and 34.9 MPa after 7 days, see Fig. 5. The strength development agrees with the formation of C_2AH_8 and C_4AH_{19}, which were found after 24 h in samples analysed with calorimetry. From 7 days up to 28 days hydration, the compressive strength dropped 13 MPa down to 21.9 MPa, which suggests a conversion to the thermodynamically stable C_3AH_6. The result also suggests that Q-phase at this stage of the hydration has not started to form stratlingite, to any significant extent (which is reported as a hydration product of Q-phase) since the formation of C_2ASH_8 would have prevented the decline in strength. The argument also seems to hold true with regard to the amorphous phase that accounts for about 35 wt.% of the material. The blend with GGBFS reacted more slowly than neat LFS as could be expected. The strength was determined to 17.9 MPa after 2 days, and 16.4 MPa after 7 days. The strength after 28 days however, was superior to LFS by measuring 31.6 MPa. The increase in strength reflects the formation of C_2ASH_8

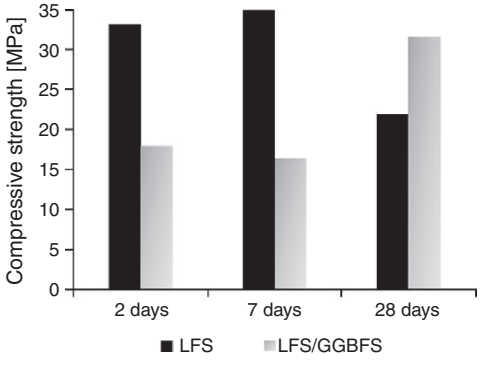

Fig. 5. Compressive strength development of mortar prisms.

which is explained by an activation of the GGBFS that was apparent already after 24 h at the same temperature (20 °C) according to Fig. 4b.

3.4. Kinetic model

The temperature dependence of the acceleration period has been examined using the Netzsch Thermokinetic software package, [20], which has also been used to propose a model that fits the experimental data. The activation energy dependence during the acceleration period, highlighted in Fig. 3, was calculated using Friedman analysis. The advancement of hydrate precipitation has been expressed as fractional degree of precipitation, α, which in turn is the ratio of heat liberated during the defined time interval for the acceleration period. In Eq. (1) for α, Q represents the heat evolved at a given time within the acceleration period and Q_i and Q_f are the initial and final values, respectively.

$$a = \frac{Q_i - Q}{Q_i - Q_f} \tag{1}$$

Friedman analysis is a model free calculation that is based on the Arrhenius equation in the form shown in Eq. (2). The software provides values for the activation energy, E_a, and the logarithm of the pre-exponential factor, ln A, without referring to any specific kinetic model which makes it advantageous to use as a first step in the approach of suggesting a specific kinetic model for a particular system.

$$ln\left(\frac{da}{dt}\right) = ln\left(\frac{A}{f(a)}\right) - \frac{E}{RT} \tag{2}$$

The results of the calculation are graphically illustrated in Fig. 6a–b. Both 100% LFS and the LFS/GGBFS blend exhibit a dependence of activation energy on the degree of hydration indicating the possibility of multiple controlling mechanisms over the duration. Therefore, the minimum apparent activation energy occurring over the whole course of the acceleration period can be considered to be most similar to the actual activation energy of chemical interaction during hydration. Friedman results for 100% LFS shows minimum activation energy of 52 kJ/mol at $\alpha \approx 0.5$ whilst the blend has a minimum of 60 kJ/mol at $\alpha \approx 0.35$. These values are comparable with a recent study concerning the hydration kinetics of CAC, [21], primarily phases CA and $C_{12}A_7$, in which an activation energy of 55 ± 5 kJ/mol was obtained at (w/c)-ratios of 0.4, 0.5 and 1, and temperatures 5–20 °C.

The LFS/GGBFS blend follows a similar trend of activation energy dependence over the course of early hydration to that of neat LFS. This leads us to come to a similar conclusion reached by Fu et al., [22] i.e. that GGBFS acts mostly as inert filler, at least at temperatures between 20 and 30 °C during early hours of the hydration, although the formation of C_2ASH_8 was proven to initiate within 24 h. The fact that the blend gives higher minimum activation energy than neat LFS can allude to the greater temperature dependence of chemical interaction in GGBFS content similar to results from Barnett et al., [23].

The data obtained from Friedman analysis were used as a complement in the determination of a rate equation that would be able to predict the relationship between fractional precipitation and time in each composition at constant temperature. The rate of diffusion during the acceleratory period of precipitation is inherently connected to the nucleation and further growth of crystals, which is why the Avrami–Erofeev model (An) was chosen for kinetic modelling of experimental data. The Avrami–Erofeev equation, Eq. (3), has been widely used in studies describing nucleation and growth.

$$f(a) = m(1-a)[-ln(1-a)]^{(m-1)/m} \tag{3}$$

Experimental data of hydrate formation is graphically represented in Fig. 7a–b along with the comparison of the Avrami–Erofeev fit for the same period of time as was assessed by Friedman analysis. The graphs have a sigmoid shape and refer to the advancement of precipitated hydrates during the defined acceleration period. The data obtained from the Avrami–Erofeev model are in agreement with the experimental data at all temperatures. The correlation coefficients for neat LFS and the blend were determined to be 0.9996 and 0.9997, respectively. The activation energies resulting from Avrami–Erofeev modelling were in good agreement with the trends from earlier Friedman analysis, 58 kJ/mol for the LFS and about 63 kJ/mol for the blend, i.e. also indicating more temperature dependence for the blend. The dimension m was 2.24

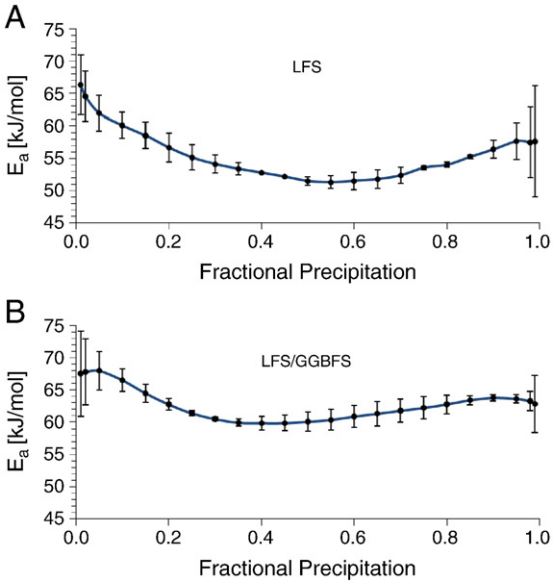

Fig. 6. a) Friedman analysis of calorimetric data in the given time interval shown in Fig. 2a. for LFS. b) Friedman analysis of calorimetric data in the given time interval shown in Fig. 2b. for blend with GGBFS.

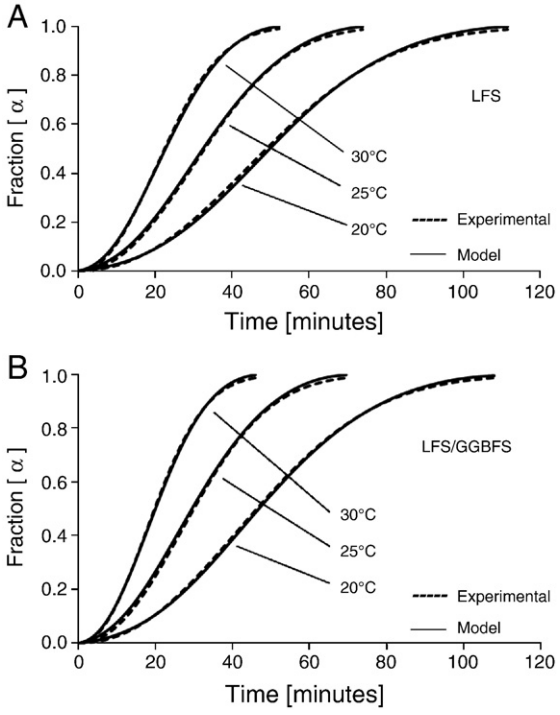

Fig. 7. a) Avrami–Erofeev fit to experimental data of LFS. b) Avrami–Erofeev fit to experimental data of LFS/GGBFS.

in case of neat LFS and 2.21 for the blend with GGBFS. The physical meaning of m is described by Eq. (4), [14]:

$$m = (p / s + q) \quad (4)$$

in which p refers to the morphology of hydrates, i.e. $p = 1$, if needles, and $p = 2$, if plates or sheets, [24]. The constant s describes the type of reaction mechanism that is occurring, i.e. $s = 1$ if phase-boundary controlled, and $s = 2$, when the rate determining step is diffusion controlled growth, [24]. Finally, q has limits at $q = 0$, if the condition of instantaneous nucleation is valid, whereas $q = 1$ when the nucleation rate is considered to be constant, [25]. Knowing that the value of m in this study should be correlated with the commonly accepted hexagonal plates of $C_2AH_8/C_2AH_{7.5}$, C_4AH_{19} and C_2ASH_8 formation (according to XRD results Fig. 4), the constant p should be set to, $p = 2$ (formation of plates/sheets). Based on the behaviour of the calorimetric curves, it is reasonable to assume the occurrence of nucleation saturation, where $q = 0$, with the argument that all nuclei are assumed to be formed instantaneously, and that growth occurs at the same rate, [25]. Under the given conditions of constants; m, p, and q the value of s should be set to, $s = 1$, meaning the reaction is phase-boundary controlled, [14]. Therefore, the rate determining step is defined as the diffusion through the boundary layer of the liquid–solid interface, [25]. An explanation for a dimension slightly >2 would be that there are phases other than calcium aluminates reacting in the slag which may affect the ongoing hydration e.g. Q-phase, β-C_2S, and thereby the result of the calculation.

4. Conclusions

- The positive influence of $C_{12}A_7$ and C_3A on the formation of C_2AH_8, $C_2AH_{7.5}$ and C_2ASH_8 shown in this study implies that LFS and the LFS/GGBFS blend may serve as a binder supplement in applications such as cold-bonded briquettes by, at the least, making important contributions to the short-term strength development (28 days) as the long term strength has yet to be determined. Furthermore, a blend containing GGBFS prevented the decline in strength experienced in specimens of neat LFS after 28 days presumably due to formation of C_2ASH_8, which according to XRD was initiated within 24 h. C_2ASH_8 is reported as a hydration product of Q-phase, but due to the decrease in strength of LFS after 28 days, it can be deduced that the formation of C_2ASH_8 through Q-phase progressed slowly as there was evidence that un-reacted contents of this phase persist after 24 h. For the same reason, it can also be stated that the short-term reactivity of the amorphous phase seems to contribute relatively limited to the strength development up to 28 days of hydration in comparison to the effect of GGBFS.
- The current results also show that the Avrami–Erofeev model may be used to help describe the sensitivity to temperature of LFS and LFS/GGBFS. The apparent activation energy of LFS was determined to be 58 kJ/mol, and 63 kJ/mol for the blend with GGBFS. The rate determining step resulting from the model was phase-boundary control at the liquid–solid interface.
- From a binder application point of view, it is important to consider the possibilities of increasing the content of calcium aluminates in the slag during processing, and to decrease the content of phases falling within the $CaO\text{-}Al_2O_3\text{-}MgO\text{-}SiO_2$ assemblage, which crystallises prior to calcium aluminates in a slowly cooled LFS, e.g. Q-phase. The latter is possible by decreasing the levels of silica and magnesia as much as possible, and to increase the use of alumina, during the refining of steel. The fact that calcium aluminates react instantaneously with water also implies that it is important to reconsider the method of slag handling, specifically in terms of avoiding any exposure to weathering and/or watering of the LFS within practical limitations. The need of reconsidering the slag handling in order to obtain a better usefulness of LFS is the subject of a forthcoming paper.

Acknowledgements

The present work was carried out within the Steel Research Programme at The Swedish Steel Producer's Association, as a contribution from SSAB Merox and SSAB EMEA. The Steel Research Programme was financed by the Swedish Governmental Agency for Innovation Systems (VINNOVA). The present work was also a contribution within the Centre of Advanced Mining and Metallurgy (CAMM).

References

[1] B. Raab, S. Stöber, H. Pöllmann, Investigations of the Hydration Behaviour of Pure Cement Phases by Different Synthesis Methods, in: C.H. Fentiman, R.J. Mangabhai, K.L. Scrivener (Eds.), Proceedings of the Centenary Conference, Avignon, 2008, pp. 79–92.
[2] J. Bensted, Calcium Aluminate Cements, in: J. Bensted, P. Barnes (Eds.), Structure and Performance of Cements, 2nd, E & FN Spon, London & New York, 2002, pp. 114–138, chapter 4.
[3] I. Odler, Calcium Aluminate Cement, Special Inorganic Cements, E&FN Spon, London & New York, 2000, pp. 173–201, chapter 10.
[4] J. Setién, D. Hernández, J.J. González, Characterization of ladle furnace basic slag for use as a construction material, Construction and Building Materials 23 (2009) 1788–1794.
[5] D. Adolfsson, N. Menad, E. Viggh, B. Björkman, Steelmaking slags as raw material for sulphoaluminate belite cement, Advances in cement research 19 (2007) 147–156.
[6] D. Adolfsson, N. Menad, E. Viggh, B. Björkman, Hydraulic properties of sulphoaluminate belite cement based on steelmaking slags, Advances in cement research 19 (2007) 133–138.
[7] H.F.W. Taylor, Calcium Aluminate, Expansive and Other Cements, Cement Chemistry, 2nd, Thomas Telford Publishing, London, 1997, pp. 295–321, chapter 10.
[8] R.C.C. Monteiro, F.P. Glasser, E.E. Lachowski, Crystallization of $CaO\text{-}Al_2O_3\text{-}SiO_2$ and $CaO\text{-}MO\text{-}Al_2O_3\text{-}SiO_2$ (M = Mg, Zn) glasses, Journal of Materials Science 24 (1989) 2839–2844.
[9] E. Dourdonis, V. Stivanakis, G.N. Angelopoulos, E. Chaniotakis, E. Frogoudakis, D. Papanastasiou, D.C. Papamantellos, High-alumina cement production from FeNi-ERF slag, limestone and diasporic bauxite, Cem. Concr. Res. 34 (2004) 941–947.
[10] I. Kaprálik, L. Stevula, F. Hanic, Hydration and hydraulic properties of the Q-phase in the system $CaO\text{-}Al_2O_3\text{-}MgO\text{-}H_2O$ referred to high alumina cements, Cem. Concr. Res. 19 (1989) 519–526.
[11] F.M. Lea, High-alumina Cement, The Chemistry of Cement and Concrete, 3rd, Edward Arnold (Publishers) Ltd, Great Britain, 1970, pp. 490–527, chapter 16.
[12] H.G. Midgley, P.B. Rao, Formation of stratlingite, $2CaO.SiO_2.Al_2O_3.8H_2O$, in relation to the hydration of high alumina cement, Cem. Concr. Res. 8 (1978) 169–172.
[13] P.K. Mechta, P. Persoff, Investigations on hydraulic cements from spent oil shale, Cem. Concr. Res. 10 (1980) 545–551.
[14] E.M. Gartner, J.F. Young, D. Damidot, I. Jawed, Hydration of Portland Cement, in: J. Bensted, P. Barnes, et al., (Eds.), Structure and Performance of Cements, E & FN Spon, London & New York, 2002, chapter 3, pp. 57–114.
[15] H. Pöllman, R. Wenda, M. Fylak, J. Göske, Cryo-SEM-FEG Investigations on Calcium Aluminate Cements, in: C.H. Fentiman, R.J. Mangabhai, K.L. Scrivener (Eds.), Proceedings of the Centenary Conference, Avignon, 2008, pp. 123–138.
[16] A.J. Majumdar, R.N. Edmonds, B. Singh, Hydration of Calcium Aluminates in Presence of Granulated Blast Furnace Slag, in: R.J. Mangabhai (Ed.), Calcium Aluminate Cements, E&FN Spon, 1990, pp. 259–271, chapter 19.
[17] A.J. Majumdar, B. Singh, R.N. Edmonds, Hydration of mixtures of $C_{12}A_7$ and granulated blast furnace slag, Cem. Concr. Res. 19 (1989) 848–856.
[18] C.H. Fentiman, S. Rashid, J.P. Bayoux, A. Bonin, M. Testud, The Effect of Curing Conditions on the Hydration and Strength Development in Fondu: Slag, in: R.J. Mangabhai (Ed.), Calcium Aluminate Cements, E&FN Spon, 1990, pp. 272–281, chapter 19.
[19] I.G. Richardson, G.W. Groves, The Microstructure of Blast Furnace Slag/high Alumina Cement Pastes, in: R.J. Mangabhai (Ed.), Calcium Aluminate Cements, E&FN Spon, 1990, pp. 282–293, Chapter 19.
[20] J. Opfermann, Kinetic Analysis Using Multivariate Non-linear Regression, Basic concepts, journal of thermal analysis and calorimetry, 60, 2000, pp. 641–658.
[21] N. Ukrainczyk, Kinetic modelling of calcium aluminate cement hydration, Chem. Eng. Sci. 65 (2010) 5605–5614.
[22] Y. Fu, J. Ding, J.J. Beaudoin, Temperature dependence of compressive strength of conversion-inhibited high alumina cement concrete, ACI Materials Journal 94 (1997) 540–545.
[23] S.J. Barnett, M.N. Soutsos, S.G. Millard, J.H. Bungey, Strength development of mortars containing ground granulated blast-furnace slag: effect of curing temperature and determination of apparent activation energies, Cem. Concr. Res. 36 (2006) 434–440.
[24] P.W. Brown, J. Pommersheim, G. Frohnsdorff, A kinetic model for the hydration of tricalcium silicate, Cem. Concr. Res. 15 (1985) 35–41.
[25] P.W. Brown, J. Pommersheim, M. James, G. Frohnsdorff, Kinetic modelling of kinetic processes, Cements Research Progress (1983) 245–260.